Recent advances in the nanoconfinement of Mg-related hydrogen storage materials: A minor review

Jingjing Zhang, Bing Zhang, Xiubo Xie, Cui Ni, Chuanxin Hou, Xueqin Sun, Xiaoyang Yang, Yuping Zhang, Hideo Kimura, and Wei Du

Articles you may be interested in

Pan-jun Wang, Ling-wei Ma, Xue-qun Cheng, and Xiao-gang Li, Influence of grain refinement on the corrosion behavior of metallic materials: A review, *Int. J. Miner. Metall. Mater.*, 28(2021), No. 7, pp. 1112-1126. https://doi.org/10.1007/s12613-021-2308-0

Mahmood Razzaghi, Masoud Kasiri-Asgarani, Hamid Reza Bakhsheshi-Rad, and Hamid Ghayour, *In vitro* bioactivity and corrosion of PLGA/hardystonite composite-coated magnesium-based nanocomposite for implant applications, *Int. J. Miner. Metall. Mater.*, 28(2021), No. 1, pp. 168-178. https://doi.org/10.1007/s12613-020-2072-6

Pian Zhang, Yun-hao Wu, Hao-ran Sun, Jia-qi Zhao, Zhi-ming Cheng, and Xiao-hong Kang, MnO_2/carbon nanocomposite based on silkworm excrement for high-performance supercapacitors, *Int. J. Miner. Metall. Mater.*, 28(2021), No. 10, pp. 1735-1744. https://doi.org/10.1007/s12613-021-2272-8

Yong Zhang and Rui-xuan Li, Editorial for special issue on nanostructured high-entropy materials, *Int. J. Miner. Metall. Mater.*, 27(2020), No. 10, pp. 1309-1311. https://doi.org/10.1007/s12613-020-2189-7

Zhi-yuan Feng, Wen-jie Peng, Zhi-xing Wang, Hua-jun Guo, Xin-hai Li, Guo-chun Yan, and Jie-xi Wang, Review of silicon-based alloys for lithium-ion battery anodes, *Int. J. Miner. Metall. Mater.*, 28(2021), No. 10, pp. 1549-1564. https://doi.org/10.1007/s12613-021-2335-x

Qiao-bao Zhang, Yong-chang Liu, and Xiao-bo Ji, Editorial for special issue on advanced materials for energy storage and conversion, *Int. J. Miner. Metall. Mater.*, 28(2021), No. 10, pp. 1545-1548. https://doi.org/10.1007/s12613-021-2354-7

IJMMM WeChat

QQ author group

Invited Review

Recent advances in the nanoconfinement of Mg-related hydrogen storage materials: A minor review

Jingjing Zhang, Bing Zhang, Xiubo Xie✉*, Cui Ni, Chuanxin Hou, Xueqin Sun, Xiaoyang Yang, Yuping Zhang, Hideo Kimura, and Wei Du*✉

School of Environmental and Material Engineering, Yantai University, Yantai 264005, China

Abstract: Hydrogen is an ideal clean energy because of its high calorific value and abundance of sources. However, storing hydrogen in a compact, inexpensive, and safe manner is the main restriction on the extensive utilization of hydrogen energy. Magnesium (Mg)-based hydrogen storage material is considered a reliable solid hydrogen storage material with the advantages of high hydrogen storage capacity (7.6wt%), good performance, and low cost. However, the high thermodynamic stability and slow kinetics of Mg-based hydrogen storage materials have to be overcome. In this paper, we will review the recent advances in the nanoconfinement of Mg-related hydrogen storage materials by loading Mg particles on different supporting materials, including carbons, metal–organic frameworks, and other materials. Perspectives are also provided for designing high-performance Mg-based materials using nanoconfinement.

Keywords: magnesium-based materials; hydrogen storage; nanoconfinement; carbon materials

1. Introduction

The excessive use of fossil fuels has led to concerns about environmental pollution and climate change [1–3]. Hydrogen is currently considered one of the most promising energy carriers in the future with the increasing global demand for renewable energy [4–7] because the final product is water without any other pollutants [8]. Moreover, the gravitational energy density of hydrogen is higher than other chemical fuels, making it the best choice for future energy applications to meet the requirements of global sustainability [9–12]. However, the low-cost production and safe storage of hydrogen still require to be considered to enable its wide use in daily life [13–14]. The existing field of hydrogen storage can be divided into three categories, namely, high-pressure gas, low-temperature liquid, and solid hydrogen storage [15–16]. Compared with other hydrogen storage methods, solid hydrogen storage has attracted considerable attention because of its advantages of high safety and capacity and low-energy consumption [17]. Among various solid hydrogen storage alloys and hydrides, including Ti-based [18–20], LaNi$_5$-based [21–22], hydroborons [23–25], alanates [26–28], and other novel coordination compounds [29], magnesium (Mg) is considered a reliable hydrogen storage material because of its high-weight hydrogen storage capacity, good hydrogenation/dehydrogenation reversibility, abundant resources, and cost-effectiveness in practical applications [30–36]. However, the slow absorption and desorption kinetics and high-adsorption temperature induced by Mg–H bonds limit the application of

Mg [4,37]. The addition of catalysts, such as transition metals [38–41] and their oxides [42–43], can decrease the activation energy; thus, the kinetics can be improved. However, the hydrogenation/dehydrogenation enthalpy cannot be easily changed; thus, the thermodynamic properties can hardly be modified [17,44]. Experimental and theoretical calculations have shown that when the size of the particles decreases below 10 nm, and the enthalpy change value is found to decrease after thermodynamic property tests [45–50], which leads to the conclusion that the thermodynamic properties of Mg and its hydrides vary with the size of the nanocrystals, and the absolute value of the enthalpy change decreases when the nanoparticles decrease [51–52]. The high hydrogen diffusion coefficient of the nanosized Mg particles can effectively reduce the enthalpy and enhance the hydrogen absorption and dehydrogenation dynamics [53–62]. During the hydrogen absorption and desorption cycle, the MgH$_2$ nanoparticles (NPs) without any protection tend to agglomerate and grow to larger particles. The nanoconfinement approach can effectively solve the problem of Mg-based hydride hydrogen storage materials by improving their hydrogen absorption performance [63–73]. Therefore, we review the effects of limiting Mg-based hydrogen storage materials to different nanoporous supporting materials in their properties.

2. Nanoconfinement

The nanoconfinement principle method can be described

✉ Corresponding authors: Xiubo Xie   E-mail: xiuboxie@ytu.edu.cn;   Wei Du   E-mail: duwei@ytu.edu.cn

🍎 Springer

as follows: Mg and the related ions can be easily absorbed into the pores of the obtained porous support template. Then, the clusters can be grown to larger particles, and the pores can limit the enhancement of the existing particles. In this process, the size of the materials can be effectively controlled, which can provide a good environment for further chemical reactions. The supporting materials for nanoconfinement mainly include carbon [74], metal frames [75–76], and polymer [77] materials. When NPs are restricted to nanoporous supporting materials, the particles would be stable during the cycles, and the gas–solid interface would be enhanced. Nanoconfinement can not only improve the dehydrogenation/hydrogenation performance of Mg hydrides but also prevent their agglomeration, thus leading to better cycling performance [78–80].

2.1. Methods for nanoconfinement

(1) Hydride growth *in situ* method. The hydride that needs to be filled should be deposited directly in the pores of the confined material through a certain chemical reaction. Zhang *et al.* [4] synthesized MgH_2/GR composites by mixing dibutyl magnesium and graphene in a pressure reactor, adding hydrogen pressure, and centrifuging the samples to obtain MgH_2 NPs with an average particle size of 13.8 nm, which were uniformly anchored on graphene nanosheets. Bottom-up self-assembly of MgH_2 anchored on graphene resulted in many monodisperse MgH_2 NPs (5 nm) uniformly distributed on graphene [81]. More importantly, the MgH_2 NPs do not aggregate on graphene, and the loading weight can be increased up to 75wt%, leading to an H_2 capacity of up to 5.7wt% for the entire system. With MgH_2@graphene as a "smart nanoreactor," where graphene acts as a flexible structural carrier and MgH_2 NPs act as effective nonuniform nucleation sites to adsorb $LiBH_4$ solutions, $2LiBH_4$–MgH_2 nanocomposites with a loading ratio of up to 80wt% were prepared on graphene in a controlled manner. The graphene-supported $2LiBH_4$–MgH_2 nanocomposites exhibited significantly improved hydrogen storage properties compared with other reported $2LiBH_4$–MgH_2 systems. For example, at a temperature of 623 K, the graphene-supported $2LiBH_4$–MgH_2 nanocomposite exhibited a reversible storage capacity of up to 8.9wt% H_2 after 25 cycles without degradation. The important role of graphene in improving the cycling performance of hydrogen storage materials was further confirmed [82]. Nielsen *et al.* [83] used this method to mix carbon aerogel with the heptane solution of dibutyl magnesium. After the evaporation of heptane in the glove box, dibutyl magnesium crystallized in the pores of the carbon aerogel and was deposited in the pores of the supporting material. Then, MgH_2 was produced by the reaction of dibutyl magnesium with hydrogen at a certain temperature and pressure (443 K, 5 MPa) and confined in the carbon aerogel. The hydride growth *in situ* method can effectively increase the hydride loading rate through the chemical reaction process, and hydride agglomeration can be effectively prevented during the reaction process.

(2) Melting method. During the heating process, Mg and its hydrides will melt and fill the nanopore channels of the confined material. This method is mainly based on the capillary action of the restricted material channel. De Jongh *et al.* [84] used the melting method to load Mg on porous carbon and reduced the size of Mg particles. However, with this method, the loading ratio of Mg particles on the carbon material is relatively low and needs to be improved by adding a small amount of catalyst. Because the process does not contain solvents, the subsequent handling of the material becomes easier. However, the poor wettability of the Mg-based materials on the confined material under the melting method leads to a low hydride loading rate, which often requires the addition of some catalysts to improve the situation. In the selection of inert framework materials for confined materials, the oxidation of active Mg and its hydrides in the molten state needs to be prevented [80,83].

(3) Impregnation method. In this method, the hydride is dissolved in the solvent, the selected confined material is soaked in the solution, the hydrogen storage material is loaded on the nanopore channels of the restricted material through the action of the solvent, and the solvent is evaporated through the heating process to form the desired compound [80,84]. The confinement of MgH_2 in the pore structure of metal–organic Ni scaffolds was accomplished by Ma *et al.* [75] by combining solvent thermal impregnation and wet impregnation. The activation energies for hydrogenation and dehydrogenation of the obtained composites were significantly reduced. An advantage of the impregnation method is its ease of operation; thus, it is often combined with the *in situ* growth and fusion methods.

2.2. Advantages of nanoconfinement

Various experimental results have shown that nanoconfinement can reduce the particle size of hydrides [75,84], decrease the dehydrogenation temperature [77–85], improve the reversibility of the hydrogen absorption and release processes [76,81], and reduce the activation energy of materials [77–85]. For example, de Jongh's study [84] showed that, by confining Mg particles in porous carbon, the size of Mg crystals was reduced from 5 nm to less than 2 nm. Ma *et al.* [75] prepared Ni–MOF scaffolds with a pore size of 7.58 nm, and the characteristics of these pore parameters clearly qualify it as a nanoconfinement support material, and their further experiments saw the successful synthesis of MgH_2 particles of approximately 3 nm in size on the Ni–MOF network, which also showed that the activation energies for hydrogenation and dehydrogenation of the composites obtained using the nanoconfinement methods were significantly reduced to 41.5 and 144.7 kJ/mol H_2, respectively. Moreover, in the work on graphene with nanoconfined MgH_2, Yu's group determined that many MgH_2 NPs (5 nm) were uniformly distributed on graphene, and the loading weight of MgH_2 NPs on graphene increased to 75wt% without any aggregation [81]. This is because that when the hydride particle size is effectively reduced by nanoconfinement, the hydrogen diffusion distance

is further shortened, and the number of grain boundaries also increases resulting in the diffusion paths for hydrogen atoms/molecules increase. Besides, their results also indicated that in the presence of Ni catalyst, the graphene-supported MgH_2 NPs exhibited excellent hydrogen storage performance, with their actual H_2 capacity up to 5.7wt%. Graphene/75wt% MgH_2 composites achieved complete hydrogenation and dehydrogenation at 323 and 473 K, respectively. In contrast, complete hydrogenation and dehydrogenation of MgH_2 particles required temperatures above 573 K. After 100 hydrogenation/dehydrogenation cycles, the sample showed only slight retention of capacity, but its kinetic properties still showed a high value. The emergence of graphene as a support material provides a substrate for the growth of MgH_2 NPs, while acting as a spatial barrier to further prevent the sintering and growth of MgH_2 NPs in the hydrogenation/ dehydrogenation cycle.

3. Supporting materials for nanoconfinement in magnesium-based materials

The micromorphology and hydrogen storage behavior of the constrained Mg NPs mainly depend on the porous structure of the supporting materials, and the loading weight of Mg NPs generally influences the storage capacity. Several different types of supporting materials for nanoconfinement are described in the following subsections.

3.1. Magnesium-based hydrogen storage material confined in carbon materials

Carbon materials can be effectively used as an additive or carrier for loading metal hydrides with adjustable dynamics and thermodynamic properties. Carbon materials exhibit a large specific surface area, and their porous structure is relatively stable in extreme environments. Moreover, carbon materials can act as an effective heat conductor material that facilitates heat transfer during hydride formation and decomposition [85–87]. Carbon nanotubes (CNT), carbon nanofibers (CNF), and graphene play an important role in energy utilization, the environment, and catalysis [88]. In addition to the role of the supporting material in improving the hydrogen storage performance of metal hydrides, it also provides various active sites for catalysts with catalytic effects and maintains structural stability [89].

Complex CA/MgH_2 with CA carbon aerogel as the supporting material was synthesized by Paskevicius *et al*. [90]. High-resolution images of the 5 nm dark regions in CA are shown in Fig. 1(a), and each of these dark regions shows distinct MgH_2 lattice edges. MgH_2 NPs (black dots) shown in Fig. 1(b) are distributed uniformly in the CA matrix, and their particle size is as small as 2 nm. The carbon aerogels here play two roles: first, they provide many sites for the formation of Mg and its hydrides; second, these sites are isolated so that the growth of MgH_2 particles in any direction is limited. Moreover, only a small fraction of MgH_2 NPs can form in the pores, whereas others agglomerate and form large bulk

MgH_2. Because of the inconsistent size distribution, the enthalpy and entropy for hydrogenation and dehydrogenation processes cannot be accurately measured. This attempt shows that CA can be used as a supporting material to prepare NPs.

As shown in Fig. 1(c) and (d), Jia *et al*. [91] used an ordered mesoporous carbon material as the confined material to load the MgH_2 NPs. Among the various carbon materials, CMK-3 [92] shows the best loading weight of 37.5wt%, and the particle size of MgH_2 in the carbon material is determined to be 1–2 nm. The small particle size has positive effects on the thermodynamic properties of MgH_2, resulting in a low operating temperature for hydrogen absorption, which indicates that hydrogen can be released from Mg-based hydrogen storage materials at low temperatures.

The study by Cho *et al*. [8] showed that Mg with a nanosheet structure can be obtained using a one-dimensional carbon substrate (Fig. 1(e)). The nanosheet was 3.6 nm thick. Mg with a nanosheet structure has a large specific surface area and a short diffusion path, which can accelerate hydrogen adsorption. The hydrogen absorption capacity of Mg nanosheets reached 6.0wt% without the addition of a catalyst. After loading Mg nanosheets on various one-dimensional graphite nanofibers (GNF), CNF, and CNT, the hydrogen storage performance can be further enhanced. As shown in Fig. 1(f), GNF with a fishbone structure can significantly improve the hydrogen storage performance of Mg nanosheets at high temperatures, indicating the efficacy of this unique structure. The desorption activation energy of GNF carbon-based composite significantly decreased, and this enhancement can be attributed to the interaction between the unstable edge position carbon and Mg nanosheets during the high-temperature hydrogen absorption and desorption cycle.

The MgH_2 NPs confined in the commercial carbon materials, including commercial coconut shell charcoal, multi-walled CNT, graphite, and activated carbon [74], using simple solid-phase methods, undergo complete desorption below 643 K. Coconut shell charcoal (CSC) has a typical folded nanosheet structure (Fig. 2(a)). After loading MgH_2 NPs, the smooth surfaces become rough and the particles are uniformly distributed on the sheet (Fig. 2(b)). Compared with the MgH_2@CSC composite, other composites prepared using this method exhibit obvious agglomeration and have a mold/melt boundary between MgH_2 NPs. A comparison of the hydrogen capacity of all of the composites is shown in Fig. 2(c). MgH_2@CSC composite has the highest dehydrogenation capacity among the composites, it can release about 6.3wt% of hydrogen, but others decrease to 5.5wt% (MgH_2@ CNT), 5.3wt% (MgH_2@G) and 5.1wt% (MgH_2@AC), respectively. Under the same experimental conditions, MgH_2@CSC can uptake the most hydrogen (5.4wt%) than others of the hydrogen absorption capacity. Because the fold structure can provide a large surface for the growth of nanosized Mg oxide and maintain the uniform dispersion, the MgH_2@CSC composite exhibits the best hydrogen storage performance.

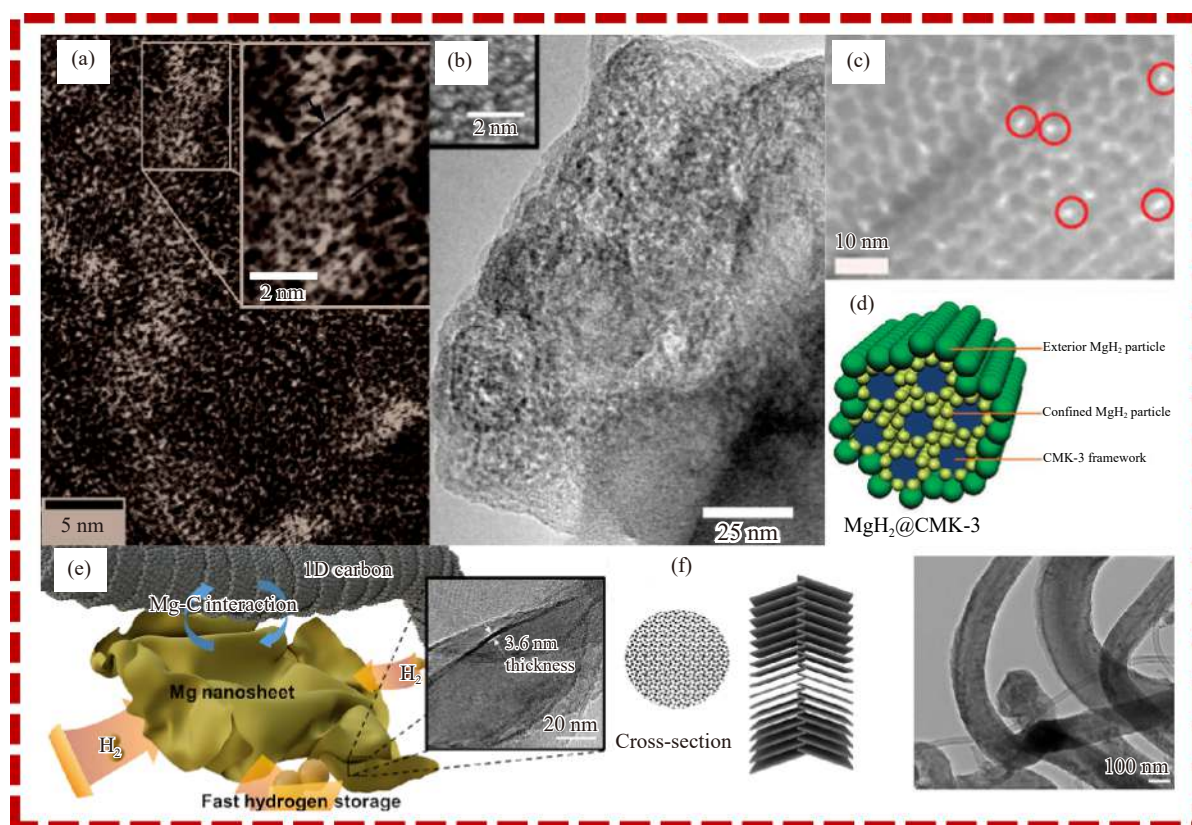Nielsen *et al*. [83] prepared MgH_2 NPs embedded in a

Fig. 1. **(a) Transmission electron microscope (TEM) micrograph of dark regions displaying MgH$_2$ lattice fringing within the carbon aerogel (CA) matrix, (b) TEM micrograph of large MgH$_2$ crystals and small MgH$_2$ particles (black dots) within the CA matrix, (c) high angle angular dark field-scanning transmission electron microscopy (HAADF-STEM) image of the restricted MgH$_2$ particles (red circles) in the 0.6MgH$_2$@CMK-3 composite sample, (d) model schematic diagram of 0.6MgH$_2$@CMK-3, (e) magnesium nanogram schematic diagram with one-dimensional (1D) carbon matrix, and (f) graphite nanofiber and its TEM. (a, b) Reprinted with permission from M. Paskevicius, H.Y. Tian, D.A. Sheppard, *et al.*, *J. Phys. Chem. C*, vol. 115, No. 5, 1757-1766 (2011) [90]. Copyright 2011 American Chemical Society. (c, d) Reproduced from Ref. [91] with permission from the Royal Society of Chemistry. (e, f) Reprinted with permission from H. Cho, S. Hyeon, H. Park, J. Kim, and E.S. Cho, *ACS Appl. Energy Mater.*, vol. 3, 8143-8149 (2020) [8]. Copyright 2020 American Chemical Society.**

nanoporous carbon aerogel composite using the infiltration method to analyze their dynamics during the hydrogenation/dehydrogenation cycles. Two different carbon aerogels were selected to load dibutyl magnesium to compare the effects of pore size on the hydrogen storage performance. By mechanical removal of excess dibutyl magnesium, the MgH$_2$ NPs can be gradually loaded on the supporting material. As shown in Fig. 2(d), the particle size confined in the X1 aerogel is determined to be 22 nm, and the filling capacity is 18.2wt%. The desorption curves shown in Fig. 2(e) indicate that X1–Mg can store 1.40wt% hydrogen, which is better than X2–Mg (0.76wt%). However, the loading rate decreases as the pores in carbons decrease, and the distribution of the pores affects the dynamics of hydrogen desorption. Moreover, the results showed that the desorption kinetics decreases with the increase in pore size. Therefore, the pore size needs to be tuned to obtain optimal performance.

In the work of Shinde's group [93], three-dimensional (3-D) structural carbon with polyhedron nanoporous network structure and well-dispersed metal coordination was synthesized. The unique 3-D carbon structure has a larger specific surface area and more abundant active edge sites than the general porous template carbon. Then, MgH$_2$ NPs are loaded to achieve uniform 3-D carbon. Fig. 2(f) and 2(g) illustrates that the particle size of Mg confined in the carbon material is approximately 5.5 nm, and the loading weight is increased to 60wt%. The prepared model diagram of the 3-D metal-modified active carbon–Mg material is shown in Fig. 2(h). The MHCH-5 composite can uptake 6.5wt% H$_2$ within 10 min (Fig. 2(i)).

In summary, carbon materials are used as nanoconfined domains. Thus, the particle size of MgH$_2$ can be significantly reduced, and the hydrogen storage kinetics can be enhanced. Compared with the ball grinding method, carbon acts as a support matrix, and its porous structure is stable during the loading process. Moreover, the morphology of carbon materials synthesized using different methods will affect the loading rate and hydrogen storage performance. Furthermore, the pore volume of the carbon material is relatively small, which limits the space for growing nanosized hydrides [94].

3.2. Magnesium-based hydrogen storage material confined in the metal–organic framework structure
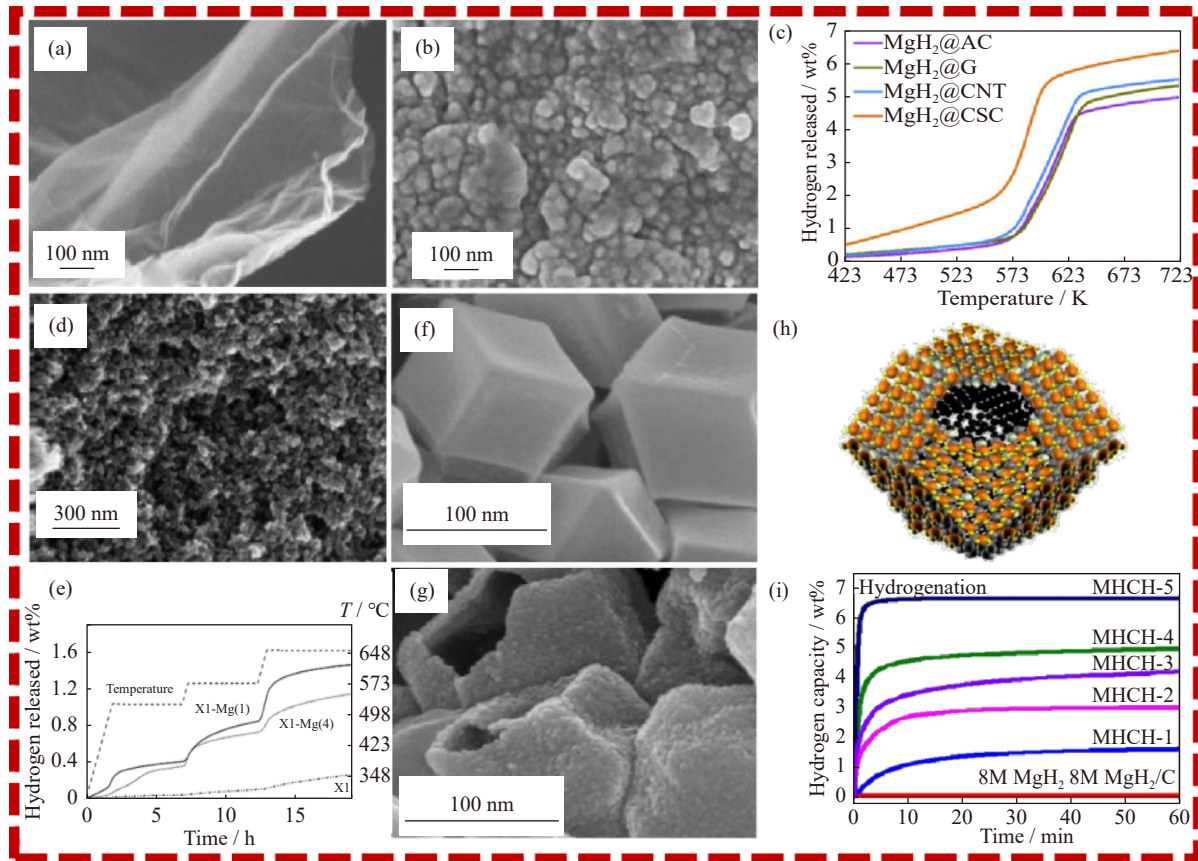
The metal–organic framework (MOF) material is a new

Fig. 2. SEM images of (a) CSC and (b) MgH$_2$@CSC, (c) composed complex H$_2$ desorption capacity curves, (d) carbon aerogels limit the morphology of Mg nanoparticles, and (e) their dehydrogenation curves. SEM images of the (f) prepared 3-D carbon and (g) MHCH-5. (h) Model diagram of active carbon–Mg materials grown *in situ* through 3D metal modification and (i) hydrogen absorption performance diagram. (a–c) Reprinted from *J. Alloys Compd.*, 825, Q.Y. Zhang, Y.K. Huang, T.C. Ma, *et al.*, Facile synthesis of small MgH$_2$ nanoparticles confined in different carbon materials for hydrogen storage, art. No. 153953, Copyright 2020, with permission from Elsevier [74]. (d, e) Reprinted with permission from T.K. Nielsen, K. Manickam, M. Hirscher, F. Besenbacher, and T.R. Jensen, *ACS Nano*, vol. 3, 3521-3528 (2009) [83]. Copyright 2009 American Chemical Society. (f–i) Reproduced from Ref. [93] with permission from the Royal Society of Chemistry.

multifunctional porous material with high porosity, large specific surface area, and structure-rich features and has been widely used in the adsorption and catalytic fields [95–99]. Chemically stable porous materials are considered ideal substrates for nanocomposites to prevent adverse reactions with highly active Mg-based compounds (such as dibutyl magnesium). MOFs with potential catalytic effects (because it contains metal ions) can be designed as a functional supporting material for Mg/MgH$_2$ nanocomposites [100]. Mg/MgH$_2$ nanoclusters can be confined in the pore structure of MOF materials, which can effectively inhibit the growth and reunion of particles.

A combination of solvent thermal and wet impregnation can be applied to produce MgH$_2$ and Mg$_2$NiH$_4$ clusters, and the reaction mechanism diagram is shown in Fig. 3(a). The nanoconfined domain of MgH$_2$ was detected in the pore structure of the metal–organic Ni scaffold, and the size of MgH$_2$ was reduced to 3 nm [75]. Meanwhile, the porous Ni-MOF shown in Fig. 3(b) acts as an "aggregation blocker" to prevent the growth and aggregation of Mg/MgH$_2$ nanocrystals during the hydrogenation/dehydrogenation cycles, thus obtaining excellent cycling stability. The unique morpholo-

gical features of Ni-MOF with a large proportion of the mesoporous interface can provide more H$_2$ dissociation/composite active and nucleation sites for Mg/MgH$_2$. This nanoconfinement method can reduce the hydrogenation enthalpy of the composite. As shown in Fig. 3(c) and (d), the activation energies for hydrogenation (41.5 kJ/mol H$_2$) and dehydrogenation (144.7 kJ/mol H$_2$) are significantly reduced, which is lower than that of pure Mg hydrogenation (92 kJ/mol H$_2$) and pure MgH$_2$ dehydrogenation (199.8 kJ/mol H$_2$) in the work.

Mg(BH$_4$)$_2$ with a high hydrogen capacity was introduced into UiO-67bpy by solvent impregnation, and the NPs were decorated on the surface of the frame material (Fig. 3(e)) [76]. As shown in Fig. 3(f), the particles are uniformly distributed in the MOF without large aggregates. This nanoconfinement method can considerably improve the hydrogen storage properties of Mg-based hydrides. Mg(BH$_4$)$_2$ can completely release hydrogen at temperatures as low as 473 K. The desorption kinetics can also be improved according to the thermodynamic measurement (Fig. 3(g)), and hydrogen is released at 393 K, approximately 423 K lower than the bulk material. The hydrogen atoms on the surface can be
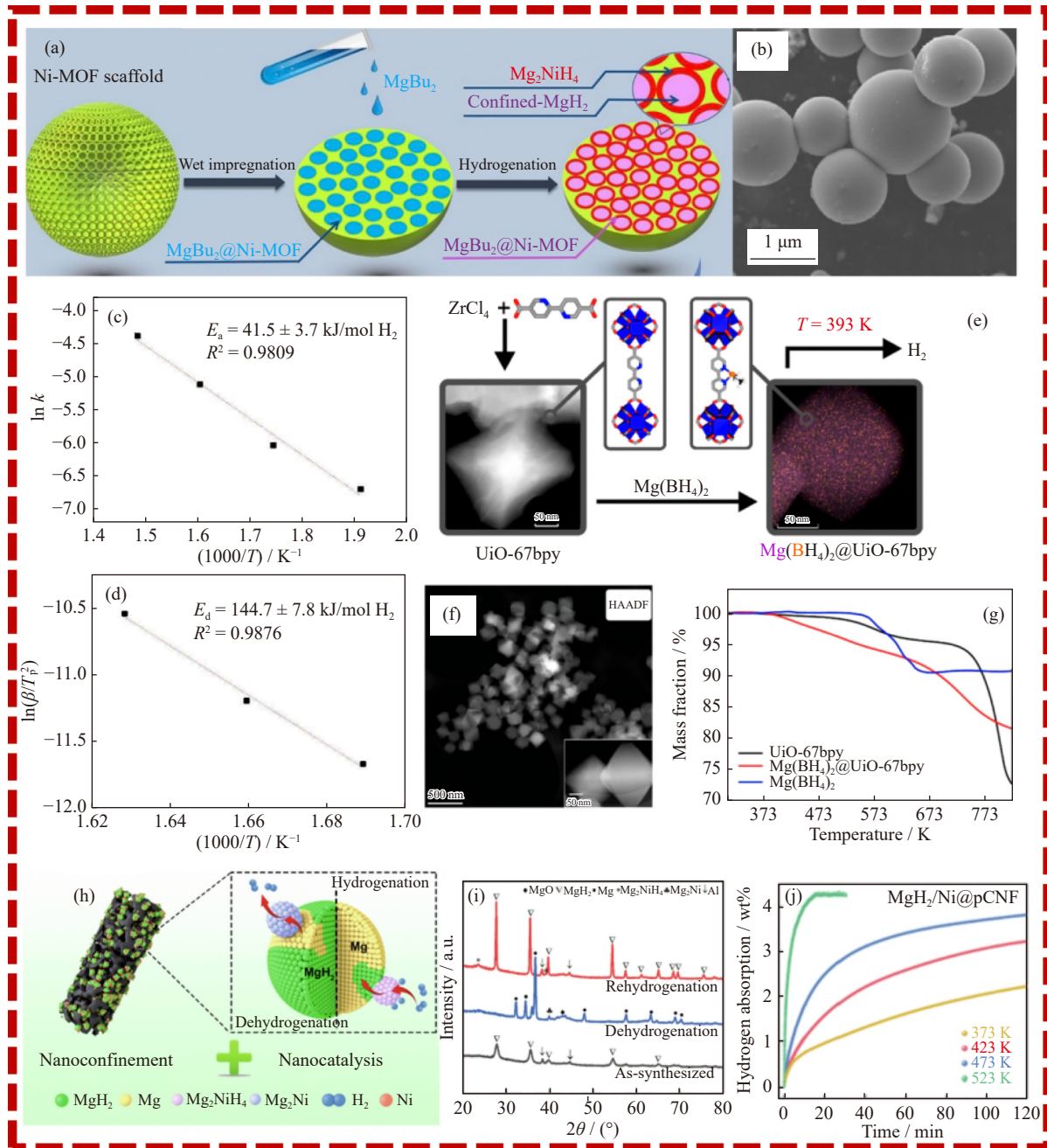
Fig. 3. (a) Nanoconfined flowchart of MgH₂ in the structure of the Ni-MOF scaffold; (b) SEM micrograph of the Ni-MOF scaffold; (c, d) Mg@Ni-MOF images of the complex activation energy (E_a, E_d) (E_a refers to the hydriding activation energy, E_d is the activation energy for the dehydrogenation process, the k in Fig. (c) is the intercept obtained from the Johnson–Mehl–Avrami–Kolmogorov (JMAK) equation, K is the temperature at isothermal hydrogen absorption (Kelvin temperature), β in Fig. (d) is the ramp-up rate in the DSC test, and T_p is the peak temperature corresponding to the DSC ramp-up rate); (e) reaction mechanism diagram of Mg(BH₄)₂@UiO-67bpy; (f) TEM diagram of Mg(BH₄)₂@UiO-67bpy (the small diagram shows two enlarged octahedral crystals); (g) TGA measurements of UiO-67bpy (black), Mg(BH₄)₂@UiO-67bpy (red), and Mg(BH₄)₂(blue); (h) synthesis mechanism diagram of MgH₂/Ni@pCNF; (i) XRD images of MgH₂/Ni@pCNF; (j) isothermal hydrogenation curves of MgH₂/Ni@pCNF at different temperatures. (a–d) Reproduced from Ref. [75] with permission from the Royal Society of Chemistry. (e–g) Reprinted with permission from A. Schneemann, L.F. Wan, A.S. Lipton, *et al.*, *ACS Nano*, vol. 14, 10294-10304 (2020) [76]. Copyright 2020 American Chemical Society. (h–j) Reprinted from *Chem. Eng. J.*, 434, L. Ren, W. Zhu, Q.Y. Zhang, *et al.*, MgH₂ confinement in MOF-derived N-doped porous carbon nanofibers for enhanced hydrogen storage, art. No. 134701, Copyright 2022, with permission from Elsevier [101].

controlled; thus, the growth of hydride in different directions can be restricted. Therefore, reversible hydrogen absorption and desorption can be eventually achieved.

Ren *et al.* [101] proposed the use of MOF-derived porous CNF, which was prepared using a combination of chemical

and physical adsorptions, as a restricted skeleton. As shown in Fig. 3(h), MgH₂/Ni NPs are thermally decomposed in the MOF to obtain MgH₂/Ni@pCNF. The X-ray diffraction pattern of MgH₂/Ni@pCNF shows that MgH₂ has a broad characteristic peak, indicating the complete hydrogenation of

MgBu$_2$ and the small grain size of MgH$_2$ (Fig. 3(i)). Because of the electron-donating ability of N atoms and the "hydrogen pump" function of Mg$_2$Ni/Mg$_2$NiH$_4$ for MgH$_2$, MgH$_2$/Ni@pCNF nanocomposites exhibit a low hydrogen absorption temperature and a high hydrogen storage capacity (4.1wt%) (Fig. 3(j)) [101].

3.3. Magnesium-based hydrogen storage material confined in the template material

A novel method for loading Mg particles in anodic aluminum oxide (AAO) template nanopore was proposed by Cui *et al.* [63]. The preparation process is systematically shown in Fig. 4(a), indicating that the Mg NPs nucleate along the AAO tube wall and generate by-products of MgO and Mg$_{17}$Al$_{12}$. The growth of Mg NPs was limited by optimizing several parameters, such as the argon flow rate, AAO template temperature, and transport distance between the Mg source and the AAO template. Under further optimization of the deposition conditions, the particle size of the loaded Mg

was less than 100 nm. Partial particles can be observed in the SEM image shown in Fig. 4(b), and the loading weight is determined to be 35wt%. The AAO template can keep the NPs stable and improve the hydrogen storage kinetics. The nanosized Mg/MgH$_2$ still showed good kinetic properties after ten dehydrogenation/hydrogenation cycles, as shown in Fig. 4 (c). The desorption entropy of MgH$_2$ was also decreased by this process.

Furthermore, MgH$_2$ particles were loaded on the mesoporous structure (MgH$_2$@CoS-NBs) using template depletion. The CoS-nanocassette (CoS-NBs) scaffold was developed as a multifunctional supporting material (Fig. 4(d)) [102]. During the confinement process, a small amount of the MgS phase was also formed *in situ* and exhibited an important catalytic role in the desorption properties. Moreover, MgS controls the growth of MgH$_2$ nanocrystals on CoS-NBs. A square shape with a rough surface can be observed in Fig. 4(e) after the addition of MgH$_2$ particles in the template. The high-resolution image shown in Fig. 4(f) indicates that
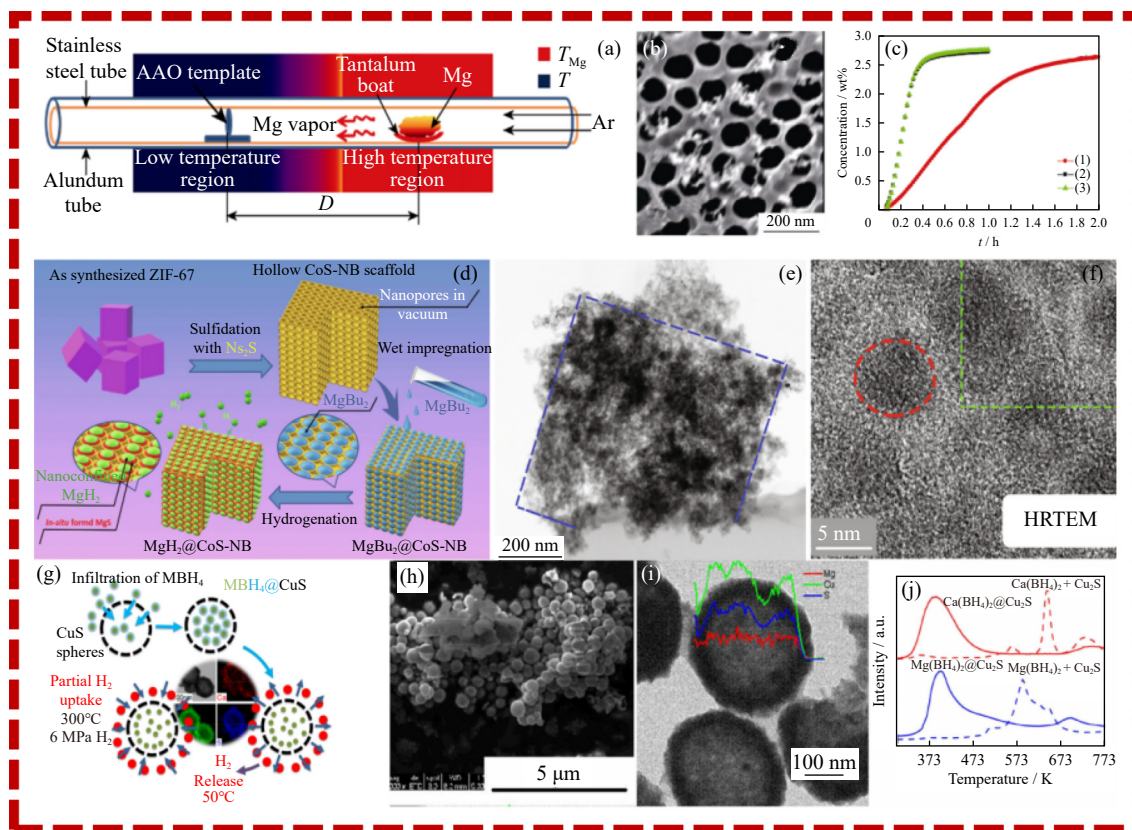

Fig. 4. (a) Schematic diagram of the process used to restrict Mg to the AAO template (T_{Mg} is the temperature of Mg vapor, *D* is the distance between the Mg vapor source and the AAO template D), (b) TEM diagram of the original AAO template cross-section, (c) isothermal dehydrogenation curve of MgH$_2$ at 573 K in the AAO template, (d) schematic diagram of the process flow of synthetic MgH$_2$@CoS-NBs composites, (e) TEM images of the MgH$_2$@CoS-NBs composites after several hydrogen cycles, (f) HRTEM micrographs of the MgH$_2$@CoS-NBs complexes after several hydrogen cycles, (g) preparation mechanism of the complex borohydrides of magnesium (Mg(BH$_4$)$_2$), (h) SEM images of Mg(BH$_4$)$_2$@Cu$_2$S, (i) TEM images of Mg(BH$_4$)$_2$@Cu$_2$S, and (j) hydrogen desorption curve of Mg(BH$_4$)$_2$@Cu$_2$S and Mg(BH$_4$)$_2$+Cu$_2$S (a physical mixture of the two substances). (a–c) Reprinted by permission from [the Nonferrous Metals Society of China and Springer-Verlag Berlin Heidelberg]: [Springer Nature] [*Rare Met.*] [Realizing nano-confinement of magnesium for hydrogen storage using vapour transport deposition, J. Cui, H. Wang, D.L. Sun, Q.G. Zhang, and M. Zhu] [Copyright 2014] [63]. (d–f) Reprinted from *Chem. Eng. J.*, 406, Z.W. Ma, S. Panda, Q.Y. Zhang, *et al.*, Improving hydrogen sorption performances of MgH$_2$ through nanoconfinement in a mesoporous CoS nano-boxes scaffold, art. No. 126790, Copyright 2020, with permission from Elsevier [102]. (g–j) Reproduced from Ref. [103] with permission from the Royal Society of Chemistry.

the diameter of the particles was approximately 5–10 nm. Its unique core/shell structure and the "nanosize effect" significantly improve the thermodynamic properties of MgH_2 by lowering the hydrogenation and dehydrogenation enthalpy [104]. The maximum hydrogen storage capacity of $MgH_2@$ CoS-NBs of 3.23wt% indicates its good loading rate for the CoS-NBs scaffold (42.5wt%).

Lai and Aguey-Zinsou [103] restricted $Mg(BH_4)_2$ to the nanopores of the Cu_2S hollow sphere, forming a complex of $Mg(BH_4)_2@Cu_2S$ (Fig. 4(g)). $Mg(BH_4)_2$ confined in hollow Cu_2S spheres generates an efficient pathway for low-temperature hydrogen diffusion. The SEM and TEM images of $Mg(BH_4)_2@Cu_2S$ shown in Fig. 4(h) and (i) confirm the existence of the $Mg(BH_4)_2$ NPs. The comparison results of the effects of the nanoconfinement method and the ordinary physical mixing method on the hydrogen storage properties are shown in Fig. 4(j). The desorption of hydrogen starts at 493 K for confined particles in Co_2S instead of 523 K for the sample obtained by the physical mixing method. Compared with the physical mixing of the hollow Cu_2S sphere with $Mg(BH_4)_2$, hydrogen is released at a temperature of 323 K, and complete hydrogen desorption is achieved below 573 K. This effect can be attributed to the instability of $Mg(BH_4)_2$ and the effect of the reduced particle size of the composite.

This proposed novel "nanoconfinement" approach can obtain superfine crystalline Mg-based materials by loading Mg on porous scaffolds [105–106]. The principal materials applied to nanocomposites can be used as structural designers, size controllers, and aggregation blockers, through which severe aggregation of nanostructured Mg/MgH_2 particles can be significantly reduced [107–109].

4. Conclusion and expectation

Magnesium hydrides with attractive potential properties, including heat resistance, high circularity, and reversibility, have been extensively investigated. Recently, nanoconfinement methods have been a popular topic for improving the kinetics and thermodynamics to improve the hydrogen storage properties of magnesium hydrides. When Mg-based materials are limited to porous materials, the reaction with the porous material can also inhibit the occurrence of some side reactions, which in turn can modulate their kinetic properties. Although the nanoconfinement method can certainly improve the hydrogen storage properties of materials, the total hydrogen storage amount of the Mg-based materials can also be affected by the choice of the framework material. For example, the existence of oxygen groups on the surface of carbon materials often causes limited reversibility when using carbon-limited materials and the possible hydroxide during the hydrogen cycle. The catalysts cannot be easily added to the composite for the high-activity reactions. For the MOF materials, how to obtain high-loading materials with easy operating parameters remains a challenge. Therefore, finding a suitable lightweight supporting material and adding an efficient catalyst should be perspectives in the future. The hydro-

gen absorption performance of hydrogen-based Mg energy storage materials can be improved once the nanoconfinement direction is organically combined with the catalyst direction under the appropriate experimental conditions.

Acknowledgements

Conflict of Interest

The authors have no conflict of interest to declare.

References

[1] Q. Wang, Y.Q. Lai, F.Y. Liu, L.X. Jiang, M. Jia, and X.L. Wang, Sb_2S_3 nanorods/porous-carbon composite from natural stibnite ore as high-performance anode for lithium-ion batteries, *Trans. Nonferrous Met. Soc. China*, 31(2021), No. 7, p. 2051.

[2] H.J. Cao, C. Pistidda, M.V. Castro Riglos, *et al*., Conversion of magnesium waste into a complex magnesium hydride system: $Mg(NH_2)_2$–LiH, *Sustainable Energy Fuels*, 4(2020), No. 4, p. 1915.

[3] X.B. Zang, L.T. Li, Z.X. Sun, *et al*., A simple physical mixing method for MnO_2/MnO nanocomposites with superior Zn^{2+} storage performance, *Trans. Nonferrous Met. Soc. China*, 30(2020), No. 12, p. 3347.

[4] B.P. Zhang, G.L. Xia, D.L. Sun, F. Fang, and X.B. Yu, Magnesium hydride nanoparticles self-assembled on graphene as anode material for high-performance lithium-ion batteries, *ACS Nano*, 12(2018), No. 4, p. 3816.

[5] Q.L. Zhu and Q. Xu, Liquid organic and inorganic chemical hydrides for high-capacity hydrogen storage, *Energy Environ. Sci.*, 8(2015), No. 2, p. 478.

[6] Z.J. Chen, K.O. Kirlikovali, K.B. Idrees, M.C. Wasson, and O.K. Farha, Porous materials for hydrogen storage, *Chem*, 8(2022), No. 3, p. 693.

[7] X. Lu, L.T. Zhang, H.J. Yu, *et al*., Achieving superior hydrogen storage properties of MgH_2 by the effect of TiFe and carbon nanotubes, *Chem. Eng. J.*, 422(2021), art. No. 130101.

[8] H. Cho, S. Hyeon, H. Park, J. Kim, and E.S. Cho, Ultrathin magnesium nanosheet for improved hydrogen storage with fishbone shaped one-dimensional carbon matrix, *ACS Appl. Energy Mater.*, 3(2020), No. 9, p. 8143.

[9] X.B. Xie, C.X. Hou, D. Wu, *et al*., Facile synthesis of various Co_3O_4/bio-activated carbon electrodes for hybrid capacitor device application, *J. Alloys Compd.*, 891(2022), art. No. 161967.

[10] Q. Luo, J.D. Li, B. Li, B. Liu, H.Y. Shao, and Q. Li, Kinetics in Mg-based hydrogen storage materials: Enhancement and mechanism, *J. Magnes. Alloys*, 7(2019), No. 1, p. 58.

[11] V. Berezovets, A. Kytsya, I. Zavaliy, and V.A. Yartys, Kinetics and mechanism of MgH_2 hydrolysis in $MgCl_2$ solutions, *Int. J. Hydrogen Energy*, 46(2021), No. 80, p. 40278.

[12] F. Tanaka, Y. Nakagawa, S. Isobe, and N. Hashimoto, Hydrogen absorption/desorption properties of light metal hydroxide systems, *Int. J. Energy Res.*, 44(2020), No. 4, p. 2941.

22

Int. J. Miner. Metall. Mater., Vol. 30, No. 1, Jan. 2023

[13] D.J. Han, K.R. Bang, H. Cho, and E.S. Cho, Effect of carbon nanoscaffolds on hydrogen storage performance of magnesium hydride, *Korean J. Chem. Eng.*, 37(2020), No. 8, p. 1306.

[14] X.L. Zhang, Y.F. Liu, X. Zhang, J.J. Hu, M.X. Gao, and H.G. Pan, Empowering hydrogen storage performance of MgH$_2$ by nanoengineering and nanocatalysis, *Mater. Today Nano*, 9(2020), art. No. 100064.

[15] N.A. Ali, N.A. Sazelee, and M. Ismail, An overview of reactive hydride composite (RHC) for solid-state hydrogen storage materials, *Int. J. Hydrogen Energy*, 46(2021), No. 62, p. 31674.

[16] T. Sadhasivam, H.T. Kim, S. Jung, S.H. Roh, J.H. Park, and H.Y. Jung, Dimensional effects of nanostructured Mg/MgH$_2$ for hydrogen storage applications: A review, *Renewable Sustainable Energy Rev.*, 72(2017), p. 523.

[17] M. Tian and C.X. Shang, Mg-based composites for enhanced hydrogen storage performance, *Int. J. Hydrogen Energy*, 44(2019), No. 1, p. 338.

[18] V.V. Berezovets, R.V. Denys, I.Y. Zavaliy, and Y.V. Kosarchyn, Effect of Ti-based nanosized additives on the hydrogen storage properties of MgH$_2$, *Int. J. Hydrogen Energy*, 47(2022), No. 11, p. 7289.

[19] S. Zholdayakova, R. Gemma, H.H. Uchida, M. Sato, and Y. Matsumura, Mechanical composition control for Ti-based hydrogen storage alloys, *e-J. Surf. Sci. Nanotechnol.*, 16(2018), p. 298.

[20] T.D. Huang, S.Y. Wu, H. Jiang, Y.P. Lu, T.M. Wang, and T.J. Li, Effect of Ti content on microstructure and properties of Ti$_x$ZrVNb refractory high-entropy alloys, *Int. J. Miner. Metall. Mater.*, 27(2020), No. 10, p. 1318.

[21] S. Chandra, P. Sharma, P. Muthukumar, and S.S.V. Tatiparti, Strategies for scaling-up LaNi$_5$-based hydrogen storage system with internal conical fins and cooling tubes, *Int. J. Hydrogen Energy*, 46(2021), No. 36, p. 19031.

[22] N.X. Zhou, M. Yamaguchi, H. Miyaoka, and Y. Kojima, Temperature rise of LaNi$_5$-based alloys by hydrogen adsorption, *Chem. Commun.*, 57(2021), No. 74, p. 9374.

[23] L. Fu, Research on battery technology of borohydride new hydrogen energy material, *IOP Conf. Ser.: Earth Environ. Sci.*, 692(2021), No. 2, art. No. 022002.

[24] Q.W. Lai, Y.W. Yang, and K.F. Aguey-Zinsou, Nanoconfinement of borohydrides in hollow carbon spheres: Melt infiltration *versus* solvent impregnation for enhanced hydrogen storage, *Int. J. Hydrogen Energy*, 44(2019), No. 41, p. 23225.

[25] J.G. Yuan, H.X. Huang, Z. Jiang, *et al.*, Ni-doped carbon nanotube-Mg(BH$_4$)$_2$ composites for hydrogen storage, *ACS Appl. Nano Mater.*, 4(2021), No. 2, p. 1604.

[26] C.A.G. Beatrice, B.R. Moreira, A.D. de Oliveira, F.R. Passador, G.R. de Almeida Neto, D.R. Leiva, and L.A. Pessan, Development of polymer nanocomposites with sodium alanate for hydrogen storage, *Int. J. Hydrogen Energy*, 45(2020), No. 8, p. 5337.

[27] N. Hosseinabadi, The beryllium/strontium doped hydrogen storage alanate nano powders for concentrating solar thermal power applications, *Int. J. Hydrogen Energy*, 46(2021), No. 7, p. 5025.

[28] K. Suárez-Alcántara, J.R. Tena-Garcia, and R. Guerrero-Ortiz, Alanates, a comprehensive review, *Materials*, 12(2019), No. 17, art. No. 2724.

[29] R. Kumar, A. Karkamkar, M. Bowden, and T. Autrey, Solid-state hydrogen rich boron-nitrogen compounds for energy storage, *Chem. Soc. Rev.*, 48(2019), No. 21, p. 5350.

[30] T.K. Nielsen, F. Besenbacher, and T.R. Jensen, Nanoconfined hydrides for energy storage, *Nanoscale*, 3(2011), No. 5, p. 2086.

[31] K. Wang, X. Zhang, Z.H. Ren, X.L. Zhang, J.J. Hu, M.X. Gao, H.G. Pan, and Y.F. Liu, Nitrogen-stimulated superior catalytic activity of niobium oxide for fast full hydrogenation of magnesium at ambient temperature, *Energy Storage Mater.*, 23(2019), p. 79.

[32] M.Y. Song and Y.J. Kwak, Hydrogenation and dehydrogenation behaviors of Mg$_2$Ni synthesized by sintering pelletized mixtures under an Ar atmosphere, *J. Nanosci. Nanotechnol.*, 19(2019), No. 10, p. 6571.

[33] P. de Rango, D. Fruchart, V. Aptukov, and N. Skryabina, Fast forging: A new SPD method to synthesize Mg-based alloys for hydrogen storage, *Int. J. Hydrogen Energy*, 45(2020), No. 14, p. 7912.

[34] J. Zhang, L. He, Y. Yao, *et al.*, Catalytic effect and mechanism of NiCu solid solutions on hydrogen storage properties of MgH$_2$, *Renewable Energy*, 154(2020), p. 1229.

[35] Z.Y. Lu, H.J. Yu, X. Lu, *et al.*, Two-dimensional vanadium nanosheets as a remarkably effective catalyst for hydrogen storage in MgH$_2$, *Rare Met.*, 40(2021), No. 11, p. 3195.

[36] X. Zhou, Z.F. Liu, F. Su, and Y.F. Fan, Magnesium composites with hybrid nano-reinforcements: 3D simulation of dynamic tensile response at elevated temperatures, *Trans. Nonferrous Met. Soc. China*, 31(2021), No. 3, p. 636.

[37] J.F. Zhang, Z.N. Li, Y.F. Wu, *et al.*, Recent advances on the thermal destabilization of Mg-based hydrogen storage materials, *RSC Adv.*, 9(2019), No. 1, p. 408.

[38] H. Yong, X. Wei, J.F. Hu, *et al.*, Influence of Fe@C composite catalyst on the hydrogen storage properties of Mg–Ce–Y based alloy, *Renewable Energy*, 162(2020), p. 2153.

[39] J.D. Li, B. Li, H.Y. Shao, W. Li, and H.J. Lin, Catalysis and downsizing in Mg-based hydrogen storage materials, *Catalysts*, 8(2018), No. 2, art. No. 89.

[40] M.D. Seo, A. Kim, and H. Jung, Co metal nanoparticles incorporated three-dimensional mesoporous graphene nanohybrids for electrochemical hydrogen storage, *J. Solid State Chem.*, 269(2019), p. 151.

[41] X.L. Yang, L. Ji, N.H. Yan, *et al.*, Superior catalytic effects of FeCo nanosheets on MgH$_2$ for hydrogen storage, *Dalton Trans.*, 48(2019), No. 33, p. 12699.

[42] J. Zhang, S. Yan, G.L. Xia, *et al.*, Stabilization of low-valence transition metal towards advanced catalytic effects on the hydrogen storage performance of magnesium hydride, *J. Magnes. Alloys*, 9(2021), No. 2, p. 647.

[43] D.M. Gattia, M. Jangir, and I.P. Jain, Study on nanostructured MgH$_2$ with Fe and its oxides for hydrogen storage applications, *J. Alloys Compd.*, 801(2019), p. 188.

[44] M. Wiesinger, B. Maitland, H. Elsen, J. Pahl, and S. Harder, Stabilizing magnesium hydride complexes with neutral ligands, *Eur. J. Inorg. Chem.*, 2019(2019), No. 41, p. 4433.

[45] S.R. Chen, R.M. Tao, C. Guo, *et al.*, A new trick for an old technology: Ion exchange syntheses of advanced energy storage and conversion nanomaterials, *Energy Storage Mater.*, 41(2021), p. 758.

[46] Y.Y. Shang, C. Pistidda, G. Gizer, T. Klassen, and M. Dornheim, Mg-based materials for hydrogen storage, *J. Magnes. Alloys*, 9(2021), No. 6, p. 1837.

[47] J.J. Liang and W.C.P. Kung, Confinement of Mg–MgH$_2$ systems into carbon nanotubes changes hydrogen sorption energetics, *J. Phys. Chem. B*, 109(2005), No. 38, p. 17837.

[48] Y.N. Liu, J.L. Zhu, Z.B. Liu, Y.F. Zhu, J.G. Zhang, and L.Q. Li, Magnesium nanoparticles with Pd decoration for hydrogen storage, *Front. Chem.*, 7(2020), art. No. 949.

[49] J. Asselin, C. Boukouvala, E.R. Hopper, Q.M. Ramasse, J.S. Biggins, and E. Ringe, Tents, chairs, tacos, kites, and rods: Shapes and plasmonic properties of singly twinned magnesium nanoparticles, *ACS Nano*, 14(2020), No. 5, p. 5968.

[50] A. Schneemann, J.L. White, S. Kang, *et al.*, Nanostructured metal hydrides for hydrogen storage, *Chem. Rev.*, 118(2018), No. 22, p. 10775.

[51] F.Y. Cheng, Z.L. Tao, J. Liang, and J. Chen, Efficient hydrogen storage with the combination of lightweight Mg/MgH$_2$ and nanostructures, *Chem. Commun.*, 48(2012), No. 59, p. 7334.

[52] C.Q. Zhou, C.D. Hu, Y.T. Li, and Q.A. Zhang, Crystallite growth characteristics of Mg during hydrogen desorption of MgH$_2$, *Prog. Nat. Sci. Mater. Int.*, 30(2020), No. 2, p. 246.

[53] Q. Li, Y.F. Lu, Q. Luo, *et al.*, Thermodynamics and kinetics of hydriding and dehydriding reactions in Mg-based hydrogen storage materials, *J. Magnes. Alloys*, 9(2021), No. 6, p. 1922.

[54] Q. Li, X. Lin, Q. Luo, *et al.*, Kinetics of the hydrogen absorption and desorption processes of hydrogen storage alloys: A review, *Int. J. Miner. Metall. Mater.*, 29(2022), No. 1, p. 32.

[55] F.M. Nyahuma, L.T. Zhang, M.Y. Song, *et al.*, Significantly improved hydrogen storage behaviors in MgH$_2$ with Nb nanocatalyst, *Int. J. Miner. Metall. Mater.*, 29(2022), No. 9, p. 1788.

[56] Y. Jia, C.H. Sun, S.H. Shen, J. Zou, S.S. Mao, and X.D. Yao, Combination of nanosizing and interfacial effect: Future perspective for designing Mg-based nanomaterials for hydrogen storage, *Renewable Sustainable Energy Rev.*, 44(2015), p. 289.

[57] Y.S. Au, Y.G. Yan, K.P. de Jong, A. Remhof, and P.E. de Jongh, Pore confined synthesis of magnesium boron hydride nanoparticles, *J. Phys. Chem. C*, 118(2014), No. 36, p. 20832.

[58] Z.Y. Han, M.L. Yeboah, R.Q. Jiang, X.Y. Li, and S.X. Zhou, Hybrid activation mechanism of thermal annealing for hydrogen storage of magnesium based on experimental evidence and theoretical validation, *Appl. Surf. Sci.*, 504(2020), art. No. 144491.

[59] Z. Ding, H. Li, and L. Shaw, New insights into the solid-state hydrogen storage of nanostructured LiBH$_4$–MgH$_2$ system, *Chem. Eng. J.*, 385(2020), art. No. 123856.

[60] Z.F. Wu, B. Tan, W.P. Lustig, *et al.*, Magnesium based coordination polymers: Syntheses, structures, properties and applications, *Coord. Chem. Rev.*, 399(2019), art. No. 213025.

[61] K.F. Aguey-Zinsou and J.R. Ares-Fernández, Hydrogen in magnesium: New perspectives toward functional stores, *Energy Environ. Sci.*, 3(2010), No. 5, p. 526.

[62] A.M. Abdalla, S. Hossain, O.B. Nisfindy, A.T. Azad, M. Dawood, and A.K. Azad, Hydrogen production, storage, transportation and key challenges with applications: A review, *Energy Convers. Manage.*, 165(2018), p. 602.

[63] J. Cui, H. Wang, D.L. Sun, Q.A. Zhang, and M. Zhu, Realizing nano-confinement of magnesium for hydrogen storage using vapour transport deposition, *Rare Met.*, 35(2016), No. 5, p. 401.

[64] H. Liu, P. Sun, R.C. Bowman Jr, Z.Z. Fang, Y. Liu, and C.S. Zhou, Effect of air exposure on hydrogen storage properties of catalyzed magnesium hydride, *J. Power Sources*, 454(2020), art. No. 227936.

[65] H.Y. Shao, L.Q. He, H.J. Lin, and H.W. Li, Progress and trends in magnesium-based materials for energy-storage research: A review, *Energy Technol.*, 6(2018), No. 3, p. 445.

[66] Y. Wang, Z.M. Ding, X.J. Li, *et al.*, Improved hydrogen storage properties of MgH$_2$ by nickel@nitrogen-doped carbon spheres, *Dalton Trans.*, 49(2020), No. 11, p. 3495.

[67] M. Lototskyy, J.M. Sibanyoni, R.V. Denys, M. Williams, B.G. Pollet, and V.A. Yartys, Magnesium-carbon hydrogen storage hybrid materials produced by reactive ball milling in hydrogen, *Carbon*, 57(2013), p. 146.

[68] M. Matsumoto, T. Kita, and K. Tanaka, Hydrogen adsorption/desorption properties of anhydrous metal oxalates; metal = Mg^{2+} and Ca^{2+}, *Bull. Chem. Soc. Jpn.*, 93(2020), No. 8, p. 985.

[69] M. Chen, Y.H. Pu, Z.Y. Li, *et al.*, Synergy between metallic components of MoNi alloy for catalyzing highly efficient hydrogen storage of MgH$_2$, *Nano Res.*, 13(2020), No. 8, p. 2063.

[70] R. Bardhan, A.M. Ruminski, A. Brand, and J.J. Urban, Magnesium nanocrystal-polymer composites: A new platform for designer hydrogen storage materials, *Energy Environ. Sci.*, 4(2011), No. 12, p. 4882.

[71] D. Mukherjee and J. Okuda, Molecular magnesium hydrides, *Angew. Chem. Int. Ed.*, 57(2018), No. 6, p. 1458.

[72] S. Cheung, W.Q. Deng, A.C.T. van Duin, and W.A. Goddard III, ReaxFF$_{MgH}$ reactive force field for magnesium hydride systems, *J. Phys. Chem. A*, 109(2005), No. 5, p. 851.

[73] J.L. White, N.A. Strange, J.D. Sugar, *et al.*, Melting of magnesium borohydride under high hydrogen pressure: Thermodynamic stability and effects of nanoconfinement, *Chem. Mater.*, 32(2020), No. 13, p. 5604.

[74] Q.Y. Zhang, Y.K. Huang, T.C. Ma, *et al.*, Facile synthesis of small MgH$_2$ nanoparticles confined in different carbon materials for hydrogen storage, *J. Alloys Compd.*, 825(2020), art. No. 153953.

[75] Z.W. Ma, Q.Y. Zhang, S. Panda, *et al., In situ* catalyzed and nanoconfined magnesium hydride nanocrystals in a Ni-MOF scaffold for hydrogen storage, *Sustainable Energy Fuels*, 4(2020), No. 9, p. 4694.

[76] A. Schneemann, L.F. Wan, A.S. Lipton, *et al.*, Nanoconfinement of molecular magnesium borohydride captured in a bipyridine-functionalized metal-organic framework, *ACS Nano*, 14(2020), No. 8, p. 10294.

[77] P.A. Song, J.F. Dai, G.R. Chen, Y.M. Yu, Z.P. Fang, W.W. Lei, S.Y. Fu, H. Wang, and Z.G. Chen, Bioinspired design of strong, tough, and thermally stable polymeric materials *via* nanoconfinement, *ACS Nano*, 12(2018), No. 9, p. 9266.

[78] D.P.E. de Jongh and D.P. Adelhelm, Nanosizing and nanoconfinement: New strategies towards meeting hydrogen storage goals, *ChemSusChem*, 3(2010), No. 12, p. 1332.

[79] L. Wang, A. Rawal, M.Z. Quadir, and K.F. Aguey-Zinsou, Nanoconfined lithium aluminium hydride (LiAlH$_4$) and hydrogen reversibility, *Int. J. Hydrogen Energy*, 42(2017), No. 20, p. 14144.

[80] X.B. Yu, Z.W. Tang, D.L. Sun, L.Z. Ouyang, and M. Zhu, Recent advances and remaining challenges of nanostructured materials for hydrogen storage applications, *Prog. Mater. Sci.*, 88(2017), p. 1.

[81] G.L. Xia, Y.B. Tan, X.W. Chen, *et al.*, Monodisperse magnesium hydride nanoparticles uniformly self-assembled on graphene, *Adv. Mater.*, 27(2015), No. 39, p. 5981.

[82] G.L. Xia, Y.B. Tan, F.L. Wu, *et al.*, Graphene-wrapped reversible reaction for advanced hydrogen storage, *Nano Energy*, 26(2016), p. 488.

[83] T.K. Nielsen, M. Manickam, M. Hirscher, F. Besenbacher, and T.R. Jensen, Confinement of MgH$_2$ nanoclusters within nanoporous aerogel scaffold materials, *ACS Nano*, 3(2009), No. 11, p. 3521.

[84] P.E. de Jongh, R.W.P. Wagemans, T.M. Eggenhuisen, *et al.*, The preparation of carbon-supported magnesium nanoparticles using melt infiltration, *Chem. Mater.*, 19(2007), No. 24, p. 6052.

[85] N.H. Yan, X. Lu, Z.Y. Lu, *et al.*, Enhanced hydrogen storage properties of Mg by the synergistic effect of grain refinement and NiTiO$_3$ nanoparticles, *J. Magnes. Alloys*, (2021). DOI: 10.1016/j.jma.2021.03.01

[86] J.H. Guo, S.J. Li, Y. Su, and G. Chen, Theoretical study of hydrogen storage by spillover on porous carbon materials, *Int. J. Hydrogen Energy*, 45(2020), No. 48, p. 25900.

[87] X.B. Xie, B.L. Wang, Y.K. Wang, C. Ni, X.Q. Sun, and W. Du, Spinel structured MFe$_2$O$_4$ (M = Fe, Co, Ni, Mn, Zn) and their composites for microwave absorption: A review, *Chem. Eng. J.*, 428(2022), art. No. 131160.

[88] T.T. le, C. Pistidda, V.H. Nguyen, *et al.*, Nanoconfinement ef-

fects on hydrogen storage properties of MgH$_2$ and LiBH$_4$, *Int. J. Hydrogen Energy*, 46(2021), No. 46, p. 23723.

[89] R.J. White, R. Luque, V.L. Budarin, J.H. Clark, and D.J. Macquarrie, Supported metal nanoparticles on porous materials. Methods and applications, *Chem. Soc. Rev.*, 38(2009), No. 2, p. 481.

[90] M. Paskevicius, H.Y. Tian, D.A. Sheppard, *et al*., Magnesium hydride formation within carbon aerogel, *J. Phys. Chem. C*, 115(2011), No. 5, p. 1757.

[91] Y. Jia, C.H. Sun, L.N. Cheng, *et al*., Destabilization of Mg–H bonding through nano-interfacial confinement by unsaturated carbon for hydrogen desorption from MgH$_2$, *Phys. Chem. Chem. Phys.*, 15(2013), No. 16, p. 5814.

[92] K.S. Xia, Q.M. Gao, C.D. Wu, S.Q. Song, and M.R. Ruan, Activation, characterization and hydrogen storage properties of the mesoporous carbon CMK-3, *Carbon*, 45(2007), No. 10, p. 1989.

[93] S.S. Shinde, D.H. Kim, J.Y. Yu, and J.H. Lee, Self-assembled air-stable magnesium hydride embedded in 3-D activated carbon for reversible hydrogen storage, *Nanoscale*, 9(2017), No. 21, p. 7094.

[94] L.M. Sanz-Moral, A. Navarrete, G. Sturm, *et al*., Release of hydrogen from nanoconfined hydrides by application of microwaves, *J. Power Sources*, 353(2017), p. 131.

[95] P. Agarwala, S.K. Pati, and L. Roy, Unravelling the possibility of hydrogen storage on naphthalene dicarboxylate-based MOF linkers: A theoretical perspective, *Mol. Phys.*, 118(2020), No. 21-22, art. No. e1757169.

[96] W.W. Sun, S.F. Li, J.F. Mao, *et al*., Nanoconfinement of lithium borohydride in Cu-MOFs towards low temperature dehydrogenation, *Dalton Trans.*, 40(2011), No. 21, p. 5673.

[97] S. Atashrouz and M. Rahmani, Predicting hydrogen storage capacity of metal–organic frameworks using group method of data handling, *Neural Comput. Appl.*, 32(2020), No. 18, p. 14851.

[98] K.K. Gangu, S. Maddila, S.B. Mukkamala, and S.B. Jonnalagadda, Characteristics of MOF, MWCNT and graphene containing materials for hydrogen storage: A review, *J. Energy Chem.*, 30(2019), p. 132.

[99] A. Salehabadi, N. Morad, and M.I. Ahmad, A study on electrochemical hydrogen storage performance of β-copper phthalocyanine rectangular nanocuboids, *Renewable Energy*, 146(2020), p. 497.

[100] A. Ahmed, Y.Y. Liu, J. Purewal, *et al*., Balancing gravimetric and volumetric hydrogen density in MOFs, *Energy Environ. Sci.*, 10(2017), No. 11, p. 2459.

[101] L. Ren, W. Zhu, Q.Y. Zhang, *et al*., MgH$_2$ confinement in MOF-derived N-doped porous carbon nanofibers for enhanced hydrogen storage, *Chem. Eng. J.*, 434(2022), art. No. 134701.

[102] Z.W. Ma, S. Panda, Q.Y. Zhang, *et al*., Improving hydrogen sorption performances of MgH$_2$ through nanoconfinement in a mesoporous CoS nano-boxes scaffold, *Chem. Eng. J.*, 406(2021), art. No. 126790.

[103] Q.W. Lai and K.F. Aguey-Zinsou, Destabilisation of Ca(BH$_4$)$_2$ and Mg(BH$_4$)$_2$ via confinement in nanoporous Cu$_2$S hollow spheres, *Sustainable Energy Fuels*, 1(2017), No. 6, p. 1308.

[104] X.B. Xie, X.J. Ma, P. Liu, J.X. Shang, X.G. Li, and T. Liu, Formation of multiple-phase catalysts for the hydrogen storage of Mg nanoparticles by adding flowerlike NiS, *ACS Appl. Mater. Interfaces*, 9(2017), No. 7, p. 5937.

[105] Y.L. Li, H. Yuan, Y.B. Chen, X.Y. Wei, K.Y. Sui, and Y.Q. Tan, Application and exploration of nanofibrous strategy in electrode design, *J. Mater. Sci. Technol.*, 74(2021), p. 189.

[106] G.Z. Li, H. Yuan, J.J. Mou, *et al*., Electrochemical detection of nitrate with carbon nanofibers and copper co-modified carbon fiber electrodes, *Compos. Commun.*, 29(2022), art. No. 101043.

[107] C.W. Duan, Y.T. Tian, X.Y. Wang, *et al*., Ni-CNTs as an efficient confining framework and catalyst for improving dehydriding/rehydriding properties of MgH$_2$, *Renewable Energy*, 187(2022), p. 417.

[108] B.G. Liu, B. Zhang, H.X. Huang, *et al*., Catalytic mechanism of *in-situ* Ni/C co-incorporation for hydrogen absorption of Mg, *J. Magnes. Alloys*, (2021). DOI: 10.1016/j.jma.2021. 08.019

[109] B. Liu, B. Zhang, X. Chen, *et al*., Remarkable enhancement and electronic mechanism for hydrogen storage kinetics of Mg nano-composite by a multi-valence Co-based catalyst, *Mater. Today Nano*, 17(2022), art. No. 100168.